Channel-coupling theory of molecular structure. Finite-element method solution for H_2^+

W. K. Ford

Xerox Webster Research Center, Xerox Square 114, Rochester, New York 14644

F. S. Levin

Physics Department, Brown University, Providence, Rhode Island 02912

The problems encountered in the channel-coupling array (CCA) calculations of the preceding paper, viz., the failure to achieve convergence and the persistence of unphysical potential-energy curves, are resolved herein with the use of the H_2^+ ion as a test case. Convergence is obtained by the use of local interpolates and the finite-element method in place of the globally defined, LCAO-type (linear combination of atomic orbitals) functions previously used. Physically correct, *ungerade* potential-energy curves result from calculations in which the *ungerade* CCA channel component wave functions are each required to vanish on the midplane normal to the symmetry axis, just like the solution to the Schrödinger equation. A proof of the foregoing property plus detailed discussions of the finite-element method and its CCA and Schrödinger-equation solutions, of spurious solutions, of convergence, and of implications of the calculations are presented.

I. INTRODUCTION

This is the fourth in a series of articles devoted to molecular structure calculations using the equations of the channel-coupling array (CCA) theory of many-body scattering.[1] In the first (hereafter I),[2] general aspects of the theory considered as a bound-state method were discussed and the results of a simple calculation for the H_2^+ ion were presented. In the second (hereafter II),[3] the same kind of approximation employed for H_2^+ was applied to the H_2 molecule. The numerical results of I and II may be summarized as follows: The approximate CCA theory was found to yield H_2^+ *gerade* and H_2 singlet potential-energy curves that were quite accurate given the crudity of the approximations, while the corresponding H_2^+ *ungerade* and H_2 triplet potential-energy curves were unphysical, since as the internucleon separation R approached zero, these latter two curves each approached $-\infty$.

The approximations used in I and II involved a one-term basis expansion, the single expansion function being the hydrogenic ground state. This function is global in character, i.e., it is defined over all of configuration or momentum space. In the preceding paper (hereafter III),[4] we presented additional results for H_2^+ and H_2 obtained by using multiterm expansions of globally defined functions, while HeH^+ was used to study the effect of channel truncation (defined in I and III). Two bases were used in the H_2^+ calculations of III; neither led to converged results nor gave an indication that enlarging the basis would lead rapidly to convergence. Furthermore, each of the multiterm H_2^+ and H_2 calculations yielded the same kind of unphysical potential energy curves described in papers I and II.

These problems of nonconvergence and unphysical results are nontrivial. They raise questions concerning the

basic many-body scattering formalism, as noted in III. Nevertheless, they are surmountable, as we demonstrate in the present paper for the case of the H_2^+ ion. Convergence is achieved by changing from an expansion basis which is global to one which is local, i.e., we use local interpolates to solve both the Schrödinger and the arrangement channel quantum mechanic[2-4] (ACQM) equations. The nonphysical (*ungerade*) results are eliminated by imposing on the wave-function components of the CCA theory a symmetry condition that in previous calculations only the full solution to the Schrödinger equation was required to obey. As remarked on in a preliminary account of this work,[5] this serves to remove any lingering doubts concerning the validity and internal consistency of the CCA procedure as applied to bound states. It also helps to confirm the power and efficiency of local interpolation methods in general[6] and the finite element method in particular.[7]

The organization of this paper is as follows. In the next section, we introduce notation and the dynamical equations, discuss the symmetry of the Schrödinger solution, and then prove that the CCA channel components vanish on the midplane normal to the interproton axis. The next section reviews the Galerkin-Petrov approach and the finite element method as we have applied it to the H_2^+ problem. In Sec. IV, we present the main results of our calculations, and the paper concludes with a brief summary and discussion in Sec. V.

II. THEORY AND SYMMETRY PROPERTIES

Our calculations have been carried out in the framework of the Born-Oppenheimer (BO) approximation.[8] Using the same notation as in III, the CCA equations for the wave-function components ψ_1 and ψ_2 are (in a.u.)

$$\begin{bmatrix} -\nabla^2/2 - r_A^{-1} & R^{-1} - r_A^{-1} \\ R^{-1} - r_B^{-1} & -\nabla^2/2 - r_B^{-1} \end{bmatrix} \begin{bmatrix} \psi_1 \\ \psi_2 \end{bmatrix} = E \begin{bmatrix} \psi_1 \\ \psi_2 \end{bmatrix}, \quad (2.1)$$

where $\vec{r}_A$ ($\vec{r}_B$) is the position coordinate of the electron relative to proton A (B), $R = |\vec{r}_A - \vec{r}_B|$, and $-\nabla^2/2$ is the electron kinetic energy operator. Arrangement channel (1) denotes an asymptotic configuration consisting of the hydrogen atom (A,e) and the bare (noninteracting) proton B. Channel (2) is obtained from channel (1) by interchanging protons A and B.

In matrix form (2.1) reads

$$\begin{bmatrix} H_1 & V^2 \\ V^1 & H_2 \end{bmatrix} \begin{bmatrix} \psi_1 \\ \psi_2 \end{bmatrix} = E \begin{bmatrix} \psi_1 \\ \psi_2 \end{bmatrix} \quad (2.2)$$

or equivalently

$$\underline{H}\,\vec{\psi} = E\vec{\psi} , \quad (2.3)$$

where H_i (V^i) is the Hamiltonian (interaction) in channel i, exactly as in III.

Exact solutions of (2.1) or (2.2) yield either the exact Schrödinger wave function Ψ via $\Psi = \psi_1 + \psi_2$ and the corresponding eigenvalue E, or else an easily identified spurious solution given by $\psi_1 + \psi_2 = 0$. Approximate solutions of (2.1) similarly yield an approximation to Ψ and E or else a spurious solution again identifiable by the fact that the sum of the approximate wave-function components vanish.[1,2]

The Schrödinger wave function Ψ obeys

$$H\Psi = E\Psi , \quad (2.4)$$

where, in the BO approximation, the Hamiltonian is (in a.u.)

$$H = -\nabla^2/2 - r_A^{-1} - r_B^{-1} + R^{-1} . \quad (2.5)$$

Denoting by P the proton interchange operator, it follows from (2.5) that $PHP = H$, and hence that[8,9]

$$P\Psi = \pm\Psi , \quad (2.6)$$

where $+$ $(-)$ indicates gerade (ungerade) states. Solutions of (2.4) can thus be labeled $\psi^\pm$, in an obvious notation.

The labeling of $\Psi^\pm$ by the superscripts $\pm$ plus the general relation $\Psi = \psi_1 + \psi_2$ means that $\psi_i \rightarrow \psi_i^\pm$:

$$\psi^\pm = \psi_1^\pm + \psi_2^\pm . \quad (2.7)$$

As discussed in III and proved in Ref. 1, we also require that

$$\psi_2^\pm = \pm P\psi_1^\pm . \quad (2.8)$$

It was shown many years ago by Burrau that an analytic solution for (2.4) can be obtained in prolate spheroidal coordinates.[10,11] Our calculations are carried out using these coordinates, our notation for which is

$$x = (r_A + r_B)/R, \quad y = (r_A - r_B)/R, \quad \phi ,$$

where ϕ is the usual azimuthal angle and the normal ranges of x and y are $x \geq 1$ and $-1 \leq y \leq 1$. We seek solutions of (2.4) and thus of (2.1) that are axially symmetric,

i.e., that have zero as the component of angular momentum along the molecular symmetry axis. In this case, $\Psi^\pm(x,y,\phi) \rightarrow \psi^\pm(x,y)$ and $\psi_i^\pm(x,y,\phi) \rightarrow \psi_i^\pm(x,y)$, $i=1,2$. From (2.6) we then have

$$P\Psi^\pm(x,y) \equiv \Psi^\pm(x,-y) = \pm\Psi^\pm(x,y) , \quad (2.9)$$

so that for the ungerade states,[8,9] $\Psi^-(x,0)=0$. Similarly, from (2.8) we find $P\psi_1^\pm(x,y) \equiv \psi_1^\pm(x,-y) = \pm\psi_2^\pm(x,y)$. These properties have the effect of reducing the domain over which $\Psi^\pm$, $\psi_1^\pm$, and $\psi_2^\pm$ need be determined from the normal range of x and y to the strip $x \geq 1$, $0 \leq y \leq 1$.

In previous work,[2,4] the vanishing of $\Psi^-(x,0)$ was ensured in the CCA approach by the relation $\psi_2^- = -P\psi_1^-$, Eq. (2.8). For example, by using the simple ansatz $\psi_1^\pm = a^\pm \exp(-r_A)$, $\psi_2^\pm = \pm a^\pm \exp(-r_B)$, it automatically follows from (2.7) that $\Psi^- = 0$ at the midplane. Unfortunately such an ansatz leads to an unphysical CCA potential-energy curve. We know now that the source of this difficulty has been the failure to recognize that, just as $\Psi^-(x,0)=0$, so also must $\psi_i^-(x,0)=0$, a relation we shall soon establish. The requirement that $\psi_i^-(x,0)=0$ means that while ψ_1^+ may be approximated by $a^+\exp(-r_A)$, the ansatz $\psi_1^- = a^-\exp(-r_A)$ is inadmissable. Indeed, any approximation to ψ_1^- must be such that $\psi_1^-(x,0)=0$. Hence none of the previous CCA ungerade H_2^+ calculations are meaningful because of their failure to employ approximate ψ_1^- satisfying this condition.

To prove that $\psi_i^-(x,0) \neq 0$ underlies the unphysical energies $E^-(R)$, i.e., that we must impose $\psi_i^-(x,0)=0$, we use (2.8) in the form $\psi_2^-(x,y) = \psi_1^-(x,-y)$ in the first of Eqs. (2.2), which becomes

$$\begin{aligned}
E^-(R)\psi_1^-(x,y) &= H_1\psi_1^-(x,y) - V^2\psi_1^-(x,-y) \\
&= \left[K - \frac{2}{R(x+y)} \right]\psi_1^-(x,y) \\
&\quad - \left[\frac{1}{R} - \frac{2}{R(x+y)} \right]\psi_1^-(x,-y) . \quad (2.10)
\end{aligned}$$

Next, we assume that the $\psi_i^\pm$ belong to the same continuity class as the $\Psi^\pm$. Then on taking the $y \rightarrow 0$ limit in (2.10) we find

$$E^-(R)\psi_1^-(x,0) = \lim_{y \rightarrow 0}[K\psi_1^-(x,y)] - \frac{1}{R}\psi_1^-(x,0) . \quad (2.11)$$

Now $\psi_1^-(x,y)$ is a bound-state wave function and so must be well behaved for all x, y, and R. A similar comment holds for $K\psi_1^-$ because of the structure of (2.10). Let us suppose that $\psi_1^-(x,0)$ is nonzero except at a finite number of points x_α, and let us choose $x \neq x_\alpha$. Then we can divide both sides of (2.11) by $\psi_1^-(x,0)$, which leads to

$$E^-(R) = -\frac{1}{R} + F(R) , \quad (2.12)$$

where $F(R) = [K\psi_1^-(x,y)]_{y=0}/\psi_1^-(x,0)$ is well behaved as $R \rightarrow 0$. Hence on examining the small R ($R \rightarrow 0$) dependence of (2.13), we find $E^-(R \rightarrow 0) \rightarrow -R^{-1}$, which is just the unphysical behavior encountered in previous H_2^+ ungerade calculations. This $-R^{-1}$ behavior has occurred because we have assumed $\psi_1^-(x,0) \neq 0$. The only procedure

left open to us for eliminating this behavior is to require that $\psi_1^-(x,0)=0$ for all x. But if $\psi_1^-(x,0)=0$, we cannot divide Eq. (2.11) by it, and hence we now avoid the necessary conclusion that $E^-(R\to0)\to-R^{-1}$. Use of $\psi_1^-(x,0)=0$ and, by Eq. (2.8), $\psi_2^-(x,0)=0$, imposes a new boundary condition on the *ungerade* channel components. We therefore expect that this will produce $E^-(R)$ which are physically well behaved. This expectation, as we show below, is verified numerically. We note in passing that if the preceding argument is applied to *gerade* states $\psi_1^+(x,0)$, the same assumption that $\psi_1^+(x,0)\neq0$ leads now to $E^+(R\to0)\to R^{-1}$, the physically correct behavior found in all the *gerade* calculations.

III. THE FINITE-ELEMENT METHOD

Unlike the Schrödinger equation, (2.1) cannot be solved analytically and one must resort to numerical methods. The numerical procedure we employ is based on the Galerkin-Petrov approximation procedure,[12] which we now briefly review. First, a complete set of orthonormal functions $\{\vec{u}_n\}$ is introduced and an Mth-order approximation to $\vec{\psi}$ is defined via

$$\vec{\psi}\simeq\vec{\psi}^{(M)}=\sum_{n=1}^{M}a_n^{(M)}\vec{u}_n \ . \tag{3.1}$$

The $a_n^{(M)}$ and approximate eigenvalues $E^{(M)}$ are determined by solving the secular equation

$$\sum_{n=1}^{M}(\vec{u}_m\mid(\underline{H}-E^{(M)}\underline{1})\mid\vec{u}_n)a_n^{(M)}=0 \ , \tag{3.2}$$

where $\mid\vec{u}_n)$ is a column vector whose ith element is the ket $\mid u_{n,i}\rangle$ and $(\vec{u}_m\mid$ is a row vector whose jth element is the bra $\langle u_{m,j}\mid$, while the symbol $(\vec{u}_m\mid\vec{u}_n)$ denotes $\sum_j\langle u_{m,j}\mid u_{n,j}\rangle$, $\sum_j$ running over the set of channels. Since there are two channels, then there will be $2M$ eigenvalues $E_\alpha^{(M)}$, $\alpha=1,\ldots,2M$. Properties of this method are reviewed in III (see also Ref. 12).

The problems associated with choosing the $\vec{u}_n$ to be globally defined basis functions are detailed in III and summarized in Sec. I above. Among these problems is the very slow convergence one generally expects (and was realized in the calculating of III) when the global functions are Coulombic. This occurs because one needs a very large number of such functions to represent accurately the wave functions Ψ or ψ_i in that region of configuration space where the particles are strongly interacting, in contrast to the asymptotic region of configuration space. The obvious need for accurate wave functions where r_A or r_B is small suggests using some kind of local basis rather than a globally defined one. Our calculations have therefore been carried out using local interpolates as basis functions.

There are a variety of local interpolation schemes for approximating the solution of differential or integral equations. We chose to work with the finite element method (FEM).[7] Both (2.1) and (2.4) were solved with this method.

The FEM is known to provide a convenient and reliable numerical method with which to solve partial differential equations, although it has only recently been applied to quantum-mechanical problems.[7] We refer to the literature[7] for the details of the method and present below merely a summary relevant to our calculation (see also Ref. 13). First, the infinite solution domain must be truncated to a finite volume in space. We chose this volume to be an ellipsoid centered at the origin, which in prolate spheroidal coordinates becomes

$$1\le x\le x_{\max}, \ \ 0\le y\le1 \ . \tag{3.3}$$

The solutions were required to vanish along $x=x_{\max}$ in order to satisfy bound-state boundary conditions (BC). Hence $x_{\max}$ must be chosen sufficiently large that the contribution of the wave-function tail extending beyond the cutoff leads to an inconsequential correction to the total energy. Since $x_{\max}$ is dependent on R, a value of $x_{\max}$ too large will waste computational effort. A rough guide used for our calculations was

$$x_{\max}\ge2t(\ln10)R$$

for t digits of precision. Ultimately $x_{\max}$ was adjusted about this value to approximately minimize the computed energy. An alternative approach, not employed herein, would be to fit the slope of the channel components to the exponential characteristics of the bound state. This method might reduce the solution domain further and increase the accuracy of the results for the same level of approximation.

Equations (2.1) and (2.4) were next transformed to a matrix element form analogous to that of (3.2) and then discretized using the Galerkin-Petrov method. A partial integration of the kinetic energy terms was also made. The ensuing surface term was dropped due to the bound state leaving a matrix element involving only first-order derivatives and interaction terms.

The FEM is based on partitioning the domain D [defined in (3.3)] into a set of M contiguous, nonoverlapping subdomains d_e, chosen here to be triangles. The solution is interpolated between a set of N points called nodes (or knots), distributed over D. The value at each node of Ψ or of the ψ_i, together with the eigenvalues E, is the output of the calculation. The placement of the N nodes and the M subdomain is schematically represented in Fig. 1.

Triangular subdomains d_e were chosen because all required integrals can be evaluated by transforming to tri-
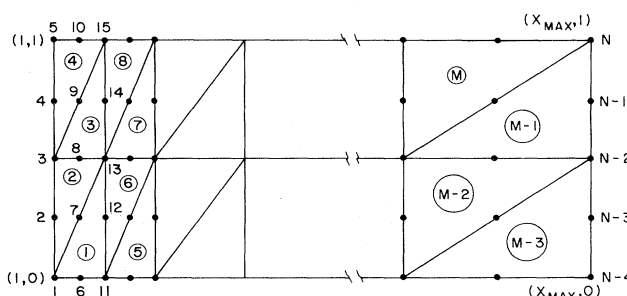

FIG. 1. Segmentation of the solution domain into elements with associated node placement.

angular coordinates $\{\zeta_1,\zeta_2,\zeta_3\}$ (see especially, Askar, Cakmak, and Rabitz[7]):

$$x = x_1\zeta_1 + x_2\zeta_2 + x_3\zeta_3$$

and   (3.4)

$$y = y_1\zeta_1 + y_2\zeta_2 + y_3\zeta_3 \;,$$

where $\zeta_1 + \zeta_2 + \zeta_3 = 1$ is imposed, making (3.4) truly a bivariate transformation. The (x_i, y_i), $i = 1,2,3$, are the coordinates of the vertices of the triangle. A typical element d_e is presented in Fig. 2, with P representing an arbitrary point (x,y) and the six nodes being labeled by their triangular coordinates. If A_e is the area of d_e, then

$$\int_{d_e} dx\, dy\, g(x,y) = 2A_e \int_0^1 d\zeta_1 \int_0^{1-\zeta_1} d\zeta_2 \tilde{g}(\zeta_1,\zeta_2,\zeta_3) \quad (3.5)$$

indicates how integrals transform, with $\tilde{g}$ denoting g as expressed in triangular coordinates. Ultimately, integrals over low-order powers of the $\{\zeta_i\}$ must be evaluated; this can be done most rapidly using the result[7]

$$\int_0^1 d\zeta_1 \int_0^{1-\zeta_1} d\zeta_2 \zeta_1^n \zeta_2^m \zeta_3^p = n!\, m!\, p!/(n+m+p+2)! \;.$$

$$(3.6)$$

In our calculations the ψ_i or Ψ were approximated on each element as a linear combination of six quadratic interpolates U_i. On a single element d_e, $\Psi(x,y)$ for example, was expressed via

$$\Psi(x,y) = \sum_{i=1}^6 \Psi_i U_i(x,y) \;, \quad\quad (3.7)$$

where in triangular coordinates the interpolates are

$$U_i = \zeta_i(2\zeta_i - 1), \quad i = 1,2,3$$

$$U_4 = 4\zeta_1\zeta_2, \quad U_5 = 4\zeta_2\zeta_3, \quad U_6 = 4\zeta_3\zeta_1 \;; \quad (3.8)$$

the ψ_i were treated in a similar fashion.

Since the interpolates share the property

$$U_i(x_j, y_j) = \delta_{ij}, \quad i,j = 1,2, \ldots, 6 \quad\quad (3.9)$$

with (x_j, y_j) denoting the nodal coordinates, the set of Ψ_i in (3.7) must equal the local values of $\Psi(x,y)$ at the six nodes on d_e. The task of assembling the global solution $\Psi(x,y)$ defined over the entire domain is accomplished by
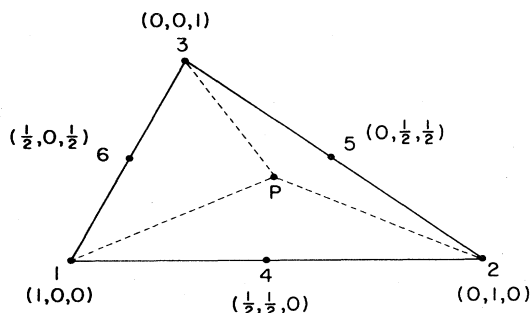

FIG. 2. Standard triangle used to define nodes and compute integrals.

keeping track of how the local node labeling corresponds to the global labeling.[7]

We note in passing that our desire to interpolate $\Psi(x,y)$ to quadratic order forced the use of six nodes and six interpolates in order to uniquely specify the solution on each element. The interaction terms were also approximated to quadratic order, following Askar *et al.*,[7] using an expression similar to (3.7). This does not reduce the precision of the calculation but simplifies the method considerably since (3.6) can then be used to evaluate all integrals. Hence the task of constructing matrix representations of (2.1) and (2.4) reduced to a matter of simple algebra and bookkeeping.

The FEM and the linear combination of atomic orbitals (LCAO) method of quantum chemistry[8,9] used in papers I—III are similar in that they each represent truncated Hilbert space expansion techniques. In the FEM the basis is formed by combining interpolates from neighboring elements; each FEM basis vector is necessarily of limited extent. In contrast, in the LCAO method, the orbitals extend globally over the entire solution domain. Furthermore, the FEM basis is nonorthogonal, as opposed to the LCAO basis. As terms are added to the LCAO calculation the requirement of orthogonality somewhat limits the choice of additional basis functions while their global definition tends to obscure the physical meaning of the subsequent calculation. In contrast, terms are added in a FEM calculation by defining new elements and nodes in the solution domain; this can be freely done to emphasize the physically important regions without the constraint of global orthogonality. Since the FEM basis is spatially compact, additional terms do not directly induce large long-range alterations in the global solution. These latter characteristics are of relatively little significance for Hermitian problems for which the Hylleraas-Undheim theorem is applicable,[14] but are of great importance for the non-Hermitian CCA-type theories, whose lack of a minimum principle may cause the approach to convergence to be uncertain when globally defined bases are used.

Convergence is obtained in the FEM by increasing the number of nodes N, and therefore the number of subdomains. In our calculations, at most 165 nodes were needed to adequately represent the channel components and wave functions in the x-y plane ($N = 165$ is a number much smaller than is customarily found in typical engineering finite element calculations[7]; this is probably due to the localized exponential aspect of the quantal bound-state wave function). The nodal points can be assigned so as to emphasize the physically important regions of D at the expense of the more inconsequential ones. As indicated in Fig. 1 we concentrated the nodes near the nuclei where the potential terms are greatest and the most significant charge density is anticipated. The formation of the entire matrix representation, including the overlap term, took just a few seconds of CPU (central processing unit) on Brown University's IBM-370/158 VM/CMS computer.

The bulk of computation time was spent determining the eigenvalues of Eqs. (2.1) and (2.4). The matrix representation of (2.1) is rank $2N$, whereas it is N for the

Schrödinger equation. However, due to the local nature of the interpolates, the matrices are extremely sparse and may be stored as banded matrices which grow in size linearly with N rather than as N^2. For N not exceeding sixty-five the full generalized eigenvalue problem (the overlap matrix was not taken as diagonal) was solved for both eigenvalues and eigenvectors using standard routines. For larger N an algorithm was developed by refining one suggested by Malik *et al.*[15] to search for the lowest-energy states. This alternative approach was warranted since only the lowest-energy solutions were desired; in addition, for the range of N used, the higher-lying states were not accurately computed: Quadratic interpolates are not sufficiently accurate for states in which the kinetic energy is large (i.e., in which there is much oscillation).

The output of the calculation was the set of energy eigenvalues and either the channel components or the wave function of the Schrödinger equation, evaluated at each nodal point in the plane. Between nodes the eigenvectors were interpolated to quadratic order using (3.7) and (3.8), leading to a piecewise continuous but not a smooth representation, since quadratic interpolates are merely dense in the space of smooth functions. That is, since only the first derivative enters into the energy function, smoothness is not required by the mathematical formulation and as a consequence the derived Galerkin sequence of solutions produces a smooth wave function only in the large-N limit. If, however, a smooth approximation is required the FEM may easily be formulated to satisfy this additional constraint.[7]

IV. RESULTS

The FEM has been applied to both the ACQM equations and the Schrödinger equation for the hydrogen molecular ion H_2^+. We find that to within the accuracy of our algorithm, the two equations gave essentially identical results for both the energy and the wave function Ψ ($=\psi_1+\psi_2$ in the CCA calculation) for N in the range $45 \leq N \leq 165$. In Table I we list the total electronic ground-state energy at the determined equilibrium internuclear separation $R_e = 2.0$ Bohr radii (a_0) as a function of the number of nodes used in the calculation. The con-

vergence is rapid with relative error of only 5×10^{-5} for the 165-node case as compared to the value of Wind,[16] who computed the H_2^+ Born-Oppenheimer energy curve beginning with the analytic solution to the Schrödinger equation. We stress that the same algorithm was applied to both the Schrödinger and ACQM equations in our calculation as a check of the validity of the method and that the results were *indistinguishable* from each other (see further comments below). Furthermore, the energy convergence of the ACQM calculation was monotonic from *above* to the exact value. These observations can be contrasted to the results of III in which the energy convergence of the LCAO calculation was very slow and began below the exact result.

In Table II the Born-Oppenheimer potential-energy curve is tabulated for the $N = 165$ ACQM calculation together with Wind's results.[16] Since the node placement was fixed for the $R = 2a_0$ case and no attempt was made to optimize this placement as R varied, the FEM ACQM calculation is necessarily most accurate near $R = 2a_0$. Nevertheless the agreement with Wind's results is exception for all R investigated. Note also that the ACQM result lies above the exact values for all values of R. Closer agreement with exact values could be attained by increasing the number of nodes or by optimizing their locations using a computer calculation rather than setting them by hand.

In order to demonstrate graphically both the rate of convergence and the R dependence of the ground-state energy for various N, we display in Fig. 3 the *gerade* results for $N = 25$, 65, and 115. On the scale of this figure, the $N = 115$ result cannot be distinguished from either the $N = 165$ result or from Wind's potential curve.

In Fig. 4 we present the computed wave-function and channel components plotted along the symmetry axis for three choices of internuclear separation. In Fig. 4(a), the channel components at $R = 3a_0$ appear somewhat like $1s$ functions but have a node on the axis toward the distant nucleus. Considering only channel (1), since channel (2) is symmetry related, the node appears at approximately $r_A = 3.7a_0$ and $r_B = 0.7a_0$. This shape persists as the nuclei are pushed toward their equilibrium separation of $R = 2.0a_0$. Channel (1) represents a situation where proton A is highly screened from proton B by the charge density of the electron localized on A. This component falls off rapidly and passes through zero near the second proton causing proton B to be poorly screened. The interac-

TABLE I. Convergence of the FEM calculation at $R = 2a_0$.

N	E
45	-0.60131
55	-0.60178
65	-0.60218
75	-0.60225
85	-0.62027
95	-0.60245
105	-0.60252
125	-0.60255
135	-0.60256
145	-0.60257
165	-0.60258
Exact[a]	-0.60263

[a]Reference 16.

TABLE II. 165-node FEM result for *gerade* energy curve.

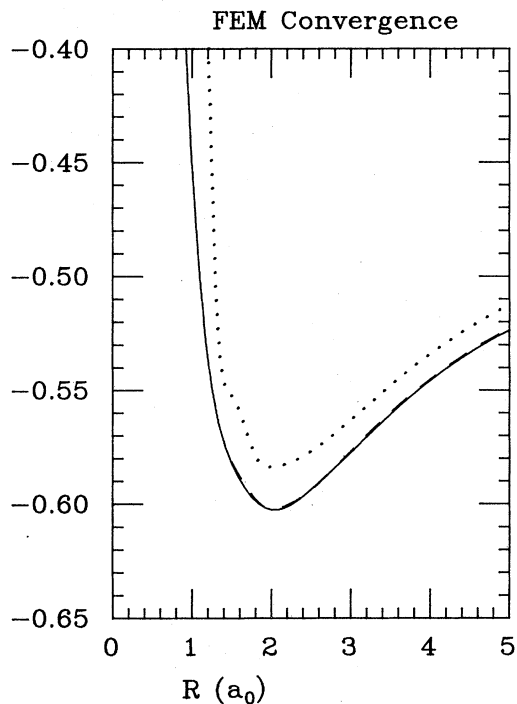| R	E_{FEM}	E_{Wind}
0.5	0.293	0.265
1.5	-0.58229	-0.58232
2.0	-0.60258	-0.60263
2.5	-0.59374	-0.59382
3.5	-0.56065	-0.56086
4.5	-0.53352	-0.53394
6.0	-0.5109	-0.5120
8.0	-0.4997	-0.5017
10.0	-0.495	-0.501

FEM Convergence

FIG. 3. Convergence of the H_2^+ ground state, *gerade*, FEM potential energy: dotted curve, $N=25$, dashed curve, $N=65$, solid curve, $N=115$.
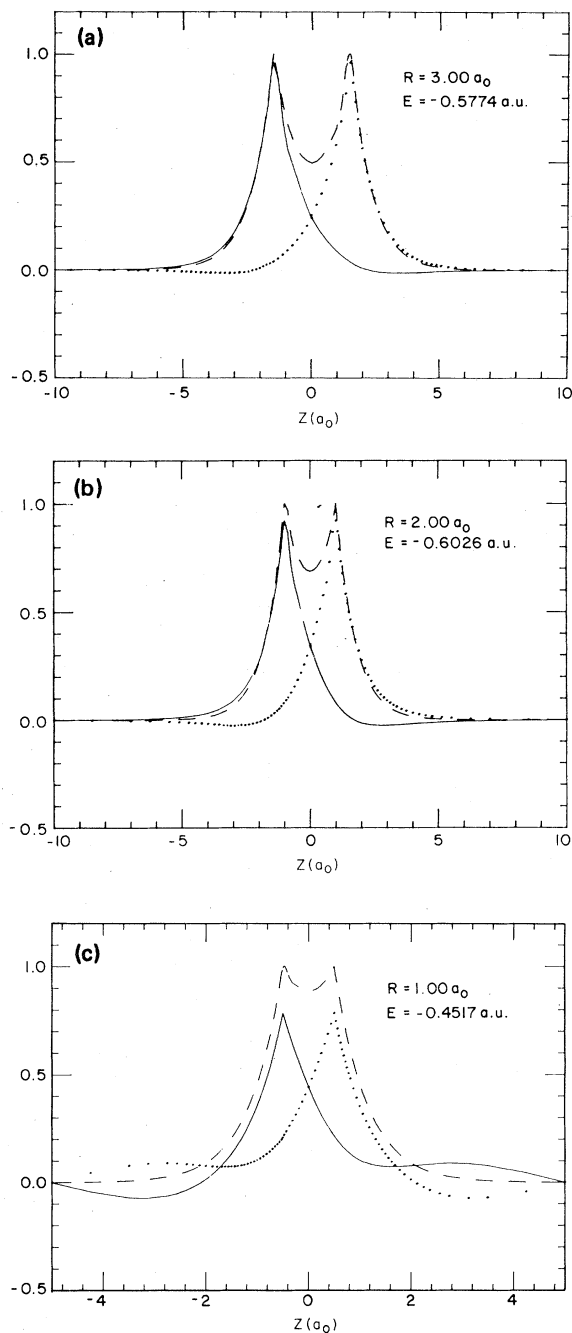

FIG. 4. CCA channel components for channels (1) (solid) and (2) (dotted), and the Schrödinger wave function (dashed), plotted along the symmetry axis for the *gerade* ground state. Internuclear separations are $3a_0$ (a), $2a_0$ (b), a_0 (c).

tion with B, however, produces a small accumulation of charge outside the internuclear region. This situation is different for $R = a_0$. The node in the channel (1) component in Fig. 4(c) has shifted considerably to $r_A = a_0$ and $r_B = 2a_0$, outside the internuclear region and in the opposite direction to the previous cases. The electronic density in channel (1) has diminished considerably near proton A and has spread out over the internuclear region. Furthermore, electronic charge has built up in each direction along the axis outside the internuclear region. Hence the protons are less shielded from each other, laying bare the internuclear repulsion, and are attracted to the increase of negative charge outside the internuclear region, enhancing their mutual repulsion. We note that for the three cases of Fig. 4, the Schrödinger wave function is qualitatively unchanged as the nuclei are brought closer, thus masking the detailed interplay of channel components and interactions which follows from use of the channel components.

It is apparent from Fig. 4 why the simple hydrogenic $1s$ state is so successful in describing the H_2^+ ground state.[2,4] The exact channel component, e.g., ψ_1^+, has a single cusp at proton A and falls off exponentially near it. Yet for the equilibrium value of R, the exact component ψ_1^+ is also smoothly varying at proton B. This implies why the single-center expansion utilized[4] in III fails to converge properly: Such an expansion does not contribute sufficiently in the region of the other center. Furthermore, the smoothness of the exact ψ_1^+ near proton B suggests that a two-center expansion using hydrogenlike basis functions may not be appropriate, since in such a basis there would be a cusp at each center.

The fact that the channel components individually exhibit more detail than the wave function is analogous to the results of Payne *et al.*[6] These authors solved the Faddeev three-body equations and found that the Faddeev wave-function components, objects analogous to our channel components, exhibit considerable oscillation even though the corresponding Schrödinger wave function does not.

Ungerade states have also been computed using the FEM. Previous LCAO calculations for the lowest-lying *ungerade* state using ACQM have proceeded by constructing an *ungerade* wave function Ψ^- from channel components ψ_1^- for which $\psi_i^-(x,0) \neq 0$. These and analogous FEM attempts produced infinitely attractive energy curves at zero internuclear separations. This is now not surprising given the discussion in Sec. II. As anticipated in Sec. II, when the additional boundary condition $\psi_i^-(x,0)=0$ was imposed, all the FEM ACQM *ungerade* results were both physically well behaved and in extremely close agreement with the FEM solutions to the Schrödinger equation; each agreed well with the analytic results of Bates *et al.*[17] for the wave functions and energy curves. In particular, the lowest ACQM *ungerade* energy curve has the correct asymptotic dissociation energy as well as being highly repulsive for small R. This latter behavior is demonstrated graphically in Fig. 5, where we compare the 1*s* *ungerade* result of I with the successful $N=165$ FEM *ungerade* calculation.

We display the channel components and wave function for the lowest-lying *ungerade* state at $R=2a_0$ in Fig. 6 where it is evident, as in the *gerade* case, that the individual channel components display considerably more variation than does the composite wave function. The channel components exhibit a long-range oscillatory nature and do not vanish smoothly at the imposed boundary. However, when added together to form the wave function the sum $\psi_1^- + \psi_2^-$ does vanish smoothly, thus satisfying the appropriate BC numerically. For larger values of R (not
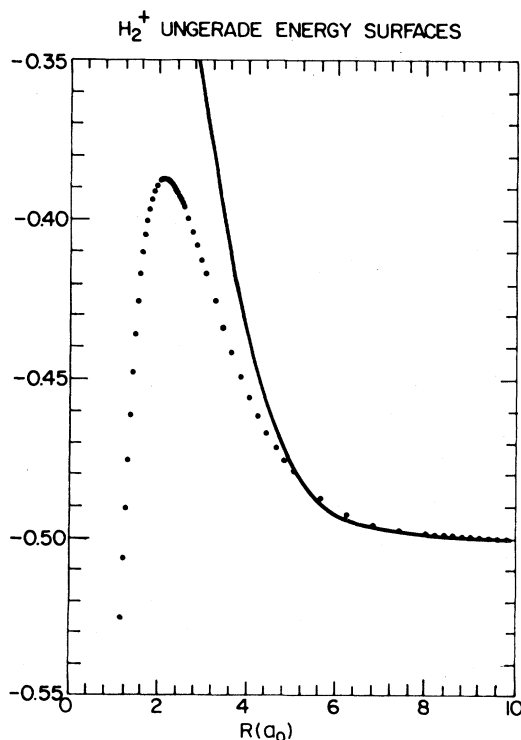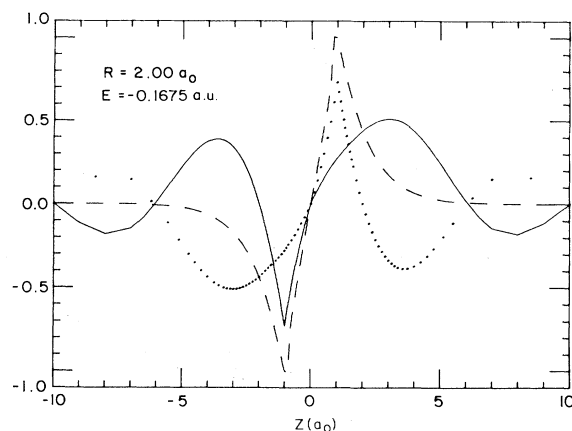

FIG. 6. Lowest H_2^+ CCA *ungerade* channel components and the Schrödinger wave function, plotted along the symmetry axis for $R=2a_0$ labeled as in Fig. 4.

shown) the oscillations of the ψ_i^- diminish and 1*s*-like components are reobtained. Thus the qualitative conclusion can be drawn that although the oscillations present in each channel are long range in character for small R, they sum to zero in the far field; furthermore, the extent of the oscillations is directly dependent on the strength of the interchannel interaction. This state, the $2p\sigma_u$ one, being unbound,[17] corresponds to a scattering state. The individual channel components reflect this fact with a high degree of charge delocalization and reduced nuclear screening as the protons are forced together.

The preceding discussion focused on the lowest *gerade* and *ungerade* states. However, an N-node FEM calculation produces N states when applied to the Schrödinger equation and $2N$ states when applied to the 2×2 ACQM matrix equation (2.1). Detailed comparison between the corresponding Schrödinger and ACQM FEM results were made for the various N up to $N=65$. It was found, for both the *gerade* and the *ungerade* cases, that exactly half, i.e., N, of the ACQM solutions were spurious. That is, N of the $\psi_i^\pm(x,y)$ were such that $\psi_1^\pm + \psi_2^\pm = 0$ for all x and y. (Their associated potential energy curves are meaningless.) The other N ACQM states were physical, i.e., their potential-energy curves displayed the proper *gerade* or *ungerade* behavior for small R. The existence of N spurious solutions is not unexpected, since only N of the $2N$ CCA solutions could possibly agree with the N Schrödinger solutions. Much to our surprise, however, for $N \geq 45$ both the *gerade* and the *ungerade*, nonspurious, CCA results agreed with those from the same FEM Schrödinger calculation to ten decimal places. This is clear and convincing numerical evidence that the spectrum of the Schrödinger equation is embedded in that of the CCA equations, as required and expected theoretically.[1,5,18] It is also evidence that a small-N FEM calculation can produce physically meaningful results even though they need not be extremely accurate. In general, for a given N, the lower-lying states we calculated were more accurate than were the higher-lying states. This is a result, noted already, of the inability of quadratic interpo-

FIG. 5. Comparison of H_2^+ lowest *ungerade* potential-energy curves: 1*s* LCAO unphysical result of Ref. 2 (dotted) and the $N=165$ FEM result obtained by imposing $\psi_i^-(x,0)=0$.

lates to represent accurately the oscillatory character of the higher-lying states, a phenomenon due to the increased kinetic energy of these states. Improvements in the energies and the ψ_i^+ of the higher-lying states could occur through use of (1) much smaller subdomains d_e and consequently many more nodes N; (2) interpolates which themselves have more curvature, e.g., cubics; (3) an extended cutoff $x_{\max}$. Each of these latter two possibilities have been verified in test calculations on the H atom.[19]

Two formal properties of the CCA theory were also investigated. The first dealt with the theoretical result that the exact, left-hand eigenstates of $\underline{H}$, i.e., the eigenstates of $\underline{H}^T$ (T stands for transpose), are independent of the channel label j and are each equal to Ψ, the Schrödinger solution at the relevant energy. This result evidently can hold only for the physical, nonspurious CCA eigenvalues. Its validity was verified in all cases for which our FEM values of E and Ψ were sufficiently accurate, as compared, for example, to the results of Bates et al.[17]

The other formal aspect we studied numerically concerned the nature of the spurious solutions. We have already commented that for $N \leq 65$, the FEM CCA solutions were equally divided between N physical and N spurious states, for both the gerade and the ungerade symmetries. This is consistent with Evan's result[18] that the spurious plus physical states span the space of eigenstates of $\underline{H}$. Furthermore, in all the cases studied, the spurious eigenvalues, for all R, were larger than the asymptotic energy -0.5 a.u., so they correspond to excited and continuum states. Finally, if $\psi_i^{(s)}$ is a spurious eigenstate of $\underline{H}$ with eigenvalue E_s, then for each E_s, the solution $\phi^{(s)}$ of $\underline{H}^T \phi^{(s)} = E_s \phi^{(s)}$ was doubly degenerate: $\phi_1^{(s)} = \phi_2^{(s)}$, with no $\phi_i^{(s)}$ being an eigenfunction of H.

V. SUMMARY AND DISCUSSION

We have established a number of results in this article. First, we have shown numerically, via the finite element method, that the physical solutions to the CCA equations for H_2^+ converge to the solutions of the Schrödinger equation. In doing so, we have also shown that the FEM is an efficient and accurate means for determining numerically the ground and excited states of a one-particle, two-center Schrödinger equation; we expect that the FEM will work as well for more complicated systems. Second, we have proved analytically that the channel components ψ_i^- for the H_2^+ ungerade states must vanish along the midplane normal to the symmetry axis, i.e., $\psi_i^-(x,0)=0$. Imposition of this condition resulted in all the FEM ungerade potential-energy curves $E^-(R)$ being physically well behaved. This therefore clears up the problem of the unphysical ungerade curves obtained in previous calculations[2,4] for which $\psi_i^-(x,0)=0$ was not imposed [indeed, when $\psi_i^-(x,0)=0$ was not imposed in our FEM ungerade calculations, the $E^-(R)$ were again unphysical, i.e., their

behavior was $E^-(R \to \infty) \to -\infty$]. We also believe that the unphysical H_2 triplet results of III can be accounted for in the same way. Current work on use of the FEM for H_2 will test this expectation; results will be reported in a future publication.

These are our two main results. They imply others. For example, the failure of our LCAO calculations to converge coupled with the success of the FEM computations means that due to the non-Hermiticity of the ACQM operator $\underline{H}$, the choice of basis expansion functions is more important than the number of terms used in the expansion. This is in contrast to the Schrödinger equation for which the Hylleraas-Undheim theorem forces a monotonic improvement regardless of the basis chosen. In this regard, it is extremely interesting that all our FEM calculations using both the CCA equations and the Schrödinger equation yielded results that converged monotonically, in contrast to the LCAO calculations of III. Given the nature of the FEM, we are not surprised at this behavior, and speculate that it will hold true for ACQM calculations in general.

The comments of the preceding paragraph notwithstanding, however, the accuracy and simplicity of the LCAO calculations of papers I–III should not be downgraded, particularly in view of our current understanding of the unphysical H_2^+ ungerade and H_2 triplet results. The ACQM equations have so far provided an excellent method for producing approximate results that are easy to obtain, relatively accurate and physically meaningful, and which, therefore, can be used to give a physical picture of the chemical bond. Because the channel structure of $\underline{H}$ yields a partitioning into asymptotically identifiable atomic or molecular fragments, ACQM is a possible basis for introducing, at a relatively high level of accuracy, an atoms-in-molecule or molecule-in-molecule description of molecular structure. This point has been remarked on before,[2,20] but takes on an added significance now that the CCA results have been shown to converge and the unphysical energy curves of I–III have been accounted for. Obviously, more (successful) approximate CCA calculations are needed in order to verify the generality of these statements. Some work along this line is in progress and will be reported on in the future.

[1]The literature on the CCA theory is now large and we cite here only the original papers plus one recent reference: M. Baer and D. J. Kouri, J. Math. Phys. **14**, 1639 (1973); D. J. Kouri and F. S. Levin, Phys. Lett. **50B**, 421 (1974); Y. Hahn, D. J. Kouri, and F. S. Levin, Phys. Lett. C **10**, 1615 (1974); W. Tobocman, *ibid*. **9**, 2466 (1974); F. S. Levin, *ibid*. **21**, 2199 (1980). As in the preceding paper (Ref. 4), we also refer herein to the CCA theory as arrangement channel quantum mechanics (ACQM).

[2]H. Krüger and F. S. Levin, Chem. Phys. Lett. **46**, 95 (1977); F. S. Levin and H. Krüger, Phys. Rev. A **15**, 2147 (1977). This latter is the first paper in this series, hereafter I.

[3]F. S. Levin and H. Krüger, Phys. Rev. A **16**, 836 (1977). This is the second paper in the series, hereafter II.

[4]W. K. Ford and F. S. Levin, preceding paper, Phys. Rev. A **29**, 30 (1984). This is the third paper in this series, hereafter III.

[5]These points have been discussed by W. K. Ford and F. S. Levin, Phys. Lett. **109B**, 155 (1982).

[6]A general discussion of local interpolation procedures can be found in P. M. Prenter, *Splines and Variational Methods* (Wiley, New York, 1975). Relevant application of spline function procedures can be found, e.g., in A. Altenberger-Siczek and T. L. Gilbert, J. Chem. Phys. **64**, 432 (1976); J. Horacek and L. Malina, Czech. J. Phys. B **27**, 1 (1977); T. A. Osborn and D. Eyre, Nucl. Phys. A **327**, 125 (1979); G. L. Payne, J. L. Friar, B. F. Gibson, and I. R. Afnan, Phys. Rev. C **22**, 823 (1980); M. Brannigan and D. Eyre (unpublished); W. Glöckle, G. Hasberg and A. R. Neghabian (unpublished). General references to the finite element method are G. Strang and G. Fix, *An Analysis of the Finite Element Method* (Prentice Hall, Englewood Cliffs, 1973), and T. J. Chung, *Finite Element Analysis in Fluid Dynamics* (McGraw-Hill, New York, 1978). Relevant applications can be found in A. Askar, J. Chem. Phys. **62**, 732 (1975); A. Askar, A. S. Cakmak, and H. A. Rabitz, Chem. Phys. **33**, 267 (1978); M. Friedman, Y. Rosenfeld, A. Rabinovitch, and R. Thieberger, J. Comp. Phys. **26**, 169 (1978); I. Kanesaka, H. Arai, and K. Kawai, Bull. Chem. Soc. Jpn. **51**, 28 (1978); M. Duff, H. Rabitz, A.

Askar, A. Cakmak, and M. Ablowitz, J. Chem. Phys. **72**, 1543 (1980); G.-D. Barg and A. Askar, Chem. Phys. Lett. **76**, 609 (1980).

[8]See, e.g., F. Pilar, *Elementary Quantum Chemistry* (McGraw-Hill, New York, 1966).

[9]See, e.g., A. C. Hurley, *Introduction to the Electron Theory of Small Molecules* (Academic, New York, 1976).

[10]Ø. Burrau, K. Dans. Vidensk. Selsk. Mat. Fys. Medd. **7**, 1 (1927); see also A. C. Hurley, Ref. 9.

[11]The Hamiltonian (2.5) is invariant under the operations of the $D_{\infty h}$ group, but $\underline{H}$ of (2.1) does not share this symmetry: It is only invariant under $C_{\infty v}$, the group of rotations about the symmetry axis. The other elements of $D_{\infty h}$, such as P, mix the two-channel components in $\underline{H}$. This fact plus the basic two-component nature of $\vec{\psi}$ are responsible for the lack of an analytic solution to (2.1).

[12]See, e.g., M. A. Krasnosel'skii, G. M. Vainikko, P. P. Zabrieko, Ya. B. Rutitskii, and V. Ya. Stetsenko, *Approximate Solutions of Operator Equations* (Wolters-Noordhoff, Groningen, 1972), or B. A. Finlayson, *The Method of Weighted Residuals and Variational Principles* (Academic, New York, 1972).

[13]W. K. Ford, Brown University Ph.D. thesis, 1980 (unpublished).

[14]For discussion and proofs of the Hylleraas-Undheim theorem see, e.g., L. Spruch, in *Lectures in Theoretical Physics,* edited by W. E. Brittin, B. W. Downs, and J. Downs (Interscience, New York, 1962), Vol. IV, p. 161, or R. G. Newton, *Scattering Theory of Waves and Particles* (McGraw-Hill, New York, 1966).

[15]D. J. Malik, J. Eccles, and D. Secrest (unpublished).

[16]H. Wind, J. Chem. Phys. **42**, 2371 (1965).

[17]D. R. Bates, K. Ledsham, and A. L. Stewart, Proc. R. Soc. London Ser. A **246**, 215 (1953).

[18]J. W. Evans, J. Math. Phys. **22**, 1672 (1981).

[19]F. S. Levin and J. Schertzer (private communication).

[20]R. Goldflam and D. J. Kouri, Chem. Phys. Lett. **34**, 594 (1974).